J Solid State Electrochem (2013) 17:911–926
DOI 10.1007/s10008-012-1977-z

REVIEW

Review and prospect of layered lithium nickel manganese oxide as cathode materials for Li-ion batteries

Shumei Dou

Received: 25 August 2012 / Revised: 8 December 2012 / Accepted: 14 December 2012 / Published online: 3 January 2013

Abstract Layered structural lithium metal oxides with rhombohedral α-$NaFeO_2$ crystal structure have been proven to be particularly suitable for application as cathode materials in lithium-ion batteries. Compared with $LiCoO_2$, lithium nickel manganese oxides are promising, inexpensive, nontoxic, and have high thermal stability; thus, they are extensively studied as alternative cathode electrode materials to the commercial $LiCoO_2$ electrode. However, a lot of work needs to be done to reduce cost and extend the effective lifetime. In this paper, the development of the layered lithium nickel manganese oxide cathode materials is reviewed from synthesis method, coating, doping to modification, lithium-rich materials, nanostructured materials, and so on, which can make electrochemical performance better. The prospects of lithium nickel manganese oxides as cathode materials for lithium-ion batteries are also looked forward to.

Keywords Lithium-ion battery · Lithium nickel manganese oxide · Review · Prospect · Electrochemical property

Introduction

During the past decades, due to the much higher energy and higher power density per unit compared to other rechargeable battery systems, lithium-ion batteries have been predominated in the portable energy storage devices. Now, they are being intensively required not only to enable the moderately charge/discharge rates applications like mobile phone and portable computer but also to meet an increasing need for new applications such as hybrid electric vehicles (HEV), plug-in hybrid electric vehicles (PHEV), and electric vehicles (EV), which need power sources with both high energy and high power density, as well as considered for stationary storage and utilization of intermittent renewable energies like solar and wind. Lithium-ion batteries for these on-going applications are depending on the cost, safety, charge/discharge rate, cycle life, energy, and power, which are mainly controlled by the components used in batteries [1, 2]. Compared to the anode materials, cathode materials have some disadvantages, such as lower capacity, more inferior cycling performance, and lesser energy density. Therefore, looking for cathode materials to be provided with elevated voltage, to have high capacity and good cycle performance, and to be safe and cheap has become one of the focus topics in recent years.

Overall, lithium-ion batteries must have five performance criteria to evaluate the cathode materials such as energy, power, life, safety, and cost as illustrated in Fig. 1 [3, 4]. First of all, energy consists of voltage and capacity. Therefore, to obtain higher energy, the cathode materials should have both high specific/volumetric capacities and high reaction voltage in the range of electrochemical stability windows of electrolytes [5, 6]. According to the previous research results, the layered structures of Li-Ni-Mn-M-O are most highly attractive due to their high energy density derived from their high operation potentials. Second, power characteristic, one of the important properties of lithium-ion batteries, is evaluated by several quantities such as rate capability, quick charging performance, and pulse power test. Meanwhile, the resistance of the cell should be reduced for rapid charge and discharge. Third, the life of the battery should be longer than that of devices operated by the batteries. Therefore, both electrode materials and the interface between electrodes and electrolyte should be more stable. Safety of lithium batteries is the fourth property which should be carefully considered from the cell material level.

S. Dou (✉)
Department of Chemistry and Chemical Engineer, Baoji University of Arts and Sciences, Baoji 721013 Shaanxi, China
e-mail: dsmwxsh@163.com

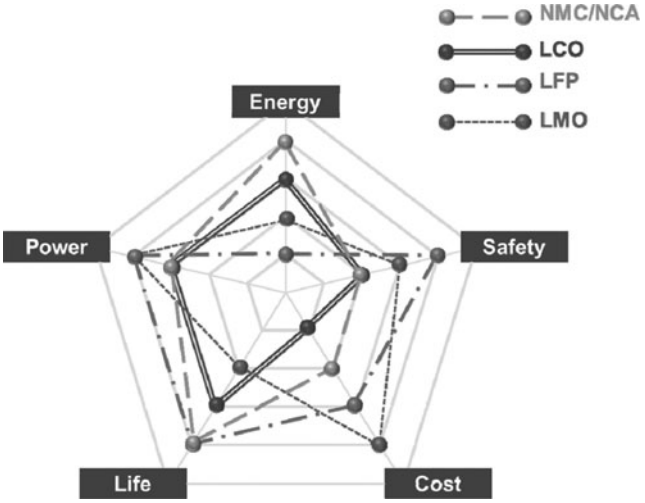

Fig. 1 Performance criteria of evaluating cathode materials. The values of each criterion were indicated for four different cathode materials. LCO=layered $LiCoO_2$, NMC=layered $LiNi_xMn_yCo_zO_2$, NCA=layered $LiNi_{1-y-z}Co_yAl_zO_2$, LMO=spinel $LiMn_2O_4$, LFP=olivine $LiFePO_4$ (copyright 2004, ACS [3]; copyright 2011, WILEY-VCH [4])

Therefore, the heat generation caused by exothermic reaction with electrolyte and oxygen evolution from cathode materials should be minimized. Last but not least, the cost of cathode materials for lithium-ion batteries should be reduced owing to the 35 % occupation of the total cost of the battery for cathode materials. As discussed above, appropriate cathode material must satisfy these five performance criteria.

$LiCoO_2$, with α-$NaFeO_2$ structure, is the earliest commercialized and most commonly used presently in lithium-ion batteries [7–9]. Although the $Li_xC_6/Li_{1-x}CoO_2$ rechargeable batteries satisfy most of the requirements discussed above, the cost, toxicity, and safety of cobalt have prevented their more widespread use. These limitations have stimulated investigation of alternative lithium-insertion electrodes [10–13]. Layered lithium nickel manganese oxides—the same structure as $LiCoO_2$, theoretical capacity of which is estimated at 274 $mAh\,g^{-1}$ under the assumption that lithium is completely delithiated, and the capacity obtained at above 200 $mAh\,g^{-1}$ practically possessing the properties such as promising, inexpensive, and nontoxic—are attracting widespread attention, becoming alternative cathode electrode materials to the commercial $LiCoO_2$ electrode used in lithium-ion batteries. In addition, the olivine-structure $LiMPO_4$ (M=Fe, Mn, Co, and Ni) [13–16] and spinel $LiM_xMn_{1-x}O_4$ (M=Fe, Ni, Co, and Cu) [17–22] have been successfully developed. For the olivine-structure series cathode materials, growing attention has been received due to the inherent stability of the polyanion group, which can delay or minimize the occurring oxygen loss. Among all the polyanion materials, $LiFePO_4$ attracts the most attention because of its excellent electrochemical properties, low cost, non-toxicity, thermal stability, and environment friendliness as well. However, the drawbacks of this material such as low energy density and poor rate capability limit its application. The energy density becomes higher than $LiFePO_4$ when the olivine structure is formed with transition metal Mn other than Fe owing to the higher potential than that of $LiFePO_4$. Nevertheless, the ionic conductivity and the electronic conductivity of $LiMnPO_4$ is much lower than that of $LiFePO_4$, making it difficult to obtain good electrochemical properties [23]. For the spinel $LiM_xMn_{1-x}O_4$ cathode materials, the largest number of studies focused on $LiNi_{0.5}Mn_{1.5}O_4$ due to its high energy density, perfect structural stability, and good cycling performance. Therefore, the spinel $LiNi_{0.5}Mn_{1.5}O_4$ is proposed to be one of very promising cathode materials for high-energy lithium-ion batteries.

Recently, there have been a lot of review articles about the lithium-ion batteries materials [24–34]. In these reviews, the lithium-ion batteries materials have been pointed out from cathode materials, anode materials, electrolyte, and so on. However, there is no article to present the layered lithium nickel manganese oxide cathode materials separately. In this paper, we systematically review the lithium nickel manganese oxide cathode materials from coating, doping to improvement of preparation, lithium-rich materials, and nanostructured materials which can make electrochemical performance better. We also look forward to the prospects of the layered lithium nickel manganese oxide for cathode materials of lithium-ion batteries. We hope that the review will give guidance to the readers for the development and perspective about lithium nickel manganese oxide cathode materials for lithium-ion batteries.

Modification of layered Li-Ni-Mn-O cathode materials

Improvement of preparation method

$LiNi_{1-x}Mn_xO_2$ was initially reported as cathode materials for lithium-ion batteries by Dahn [35]. Unfortunately, not much attention has been paid to these materials due to their poor electrochemical properties. Until 2001, both $LiNi_{0.5}Mn_{0.5}O_2$ and $Li[Ni_xLi_{(1/3-2x/3)}Mn_{(2/3-x/3)}]O_2$ synthesized above the temperature of 800 °C, reported by Ohzuku [36] and Dahn [37], respectively, showed the prominent performance of the electrochemical properties. Since then, the lithium nickel manganese oxides have caused great concerns in the academic field. Various synthesis methods such as solid-state reaction [38–42], ion exchange [40, 43], hydroxide co-precipitation method [44, 45], hydrothermal synthesis [46], and ultrasonic assistance synthesis [47] have been applied to prepare these system materials. However, the lithium nickel manganese oxides synthesized with these methods are not highly battery active due to either containing substantial Li/

Ni disorder or existing structure impurity. Recently, there are two major breakthroughs in solving those problems that is either to transform $Na(Ni_{0.5}Mn_{0.5})O_2$ into $Li(Ni_{0.5}Mn_{0.5})O_2$ by ion exchange of Na^+ for Li^+ [40, 43] or to use nickel manganese double hydroxides as precursor [38, 39]. Unfortunately, disadvantages still exist. The former is a multistep synthesis process and needs to consume large amount of salts containing Li^+. For the latter, it should be very careful to control the synthesis conditions in order to avoid the oxidation of $Mn(OH)_2$ since Mn^{2+} in nickel manganese double hydroxide is easily oxidized in air when wet. Therefore, searching for a simple and convenient method to synthesize lithium nickel manganese oxides cathode materials is very important.

Recently, Wang et al. investigated a new method to synthesis $LiNi_{0.5}Mn_{0.5}O_2$ with solid solution of $Ni_{1.5}Mn_{1.5}O_4$ as precursor prepared by means of the solid reaction between Mn $(CH_3COO)_2$ $4H_2O$ and $Ni(CH_3COO)_2$ $4H_2O$ [42]. The XRD pattern of precursor $Ni_{1.5}Mn_{1.5}O_4$ is similar to the pattern of $NiMn_2O_4$ with the Fd3m space group (Fig. 2a (a)), in which the distribution of nickel and manganese is homogeneous at the atomic level, resulting in high ordering of cations and no structural impurity in the final sample $LiNi_{0.5}Mn_{0.5}O_2$ (Fig. 2a (b)). When charged and discharged at 21.7 $mA\,g^{-1}$, this material delivers a capacity of 199 $mAh\,g^{-1}$ (Fig. 2b) and shows about 190 $mAh\,g^{-1}$ of rechargeable capacity without dramatic capacity fading during 100 cycles (Fig. 2c). They also studied the discharge capacity at different currents with cycle number (Fig. 2d) and show that the as-prepared $LiNi_{0.5}Mn_{0.5}O_2$ material has good electrochemical reversibility and structural stability. These electrochemical performances suggest that the synthesized $LiNi_{0.5}Mn_{0.5}O_2$ would be well suitable for cathode materials of high-power lithium batteries. Otherwise, they initially investigated the relationship between the ratio of I_{003}/I_{104} and capacity and found that it is almost linear. According to this relationship, the electrochemical performance of $LiNi_{0.5}Mn_{0.5}O_2$ can be conveniently judged by the ratio of I_{003}/I_{104} in XRD patterns. In addition, they studied the electrochemical properties with Co and Al doped with the solid solution method, and found that the method can be used to diversify metal that can be solid solution with Ni and Mn [48, 49].

Another breakthrough to synthesize Li-Ni-Mn-O is on a concentration-gradient cathode material [50]. In this material, each particle has a central bulk rich in Ni and a Mn-rich outer layer with decreasing Ni concentration and increasing Mn and Co concentrations as the surface, as shown in Fig. 3a. This core–shell structural material can be demonstrated by scanning electron microscopy (SEM), as illustrated in Fig. 3b. However, because of the different diffusions of Ni, Co, and Mn during the calcination at the interface between the bulk and the outer layer, the Ni-rich bulk and the outer layer are not connected closely. This shortage could bring some effects to the electrochemical properties. This core–shell structure can also be confirmed by the electron-probe X-ray microanalysis (EPAM), as revealed in Fig. 3c. The Ni, Mn, and Co

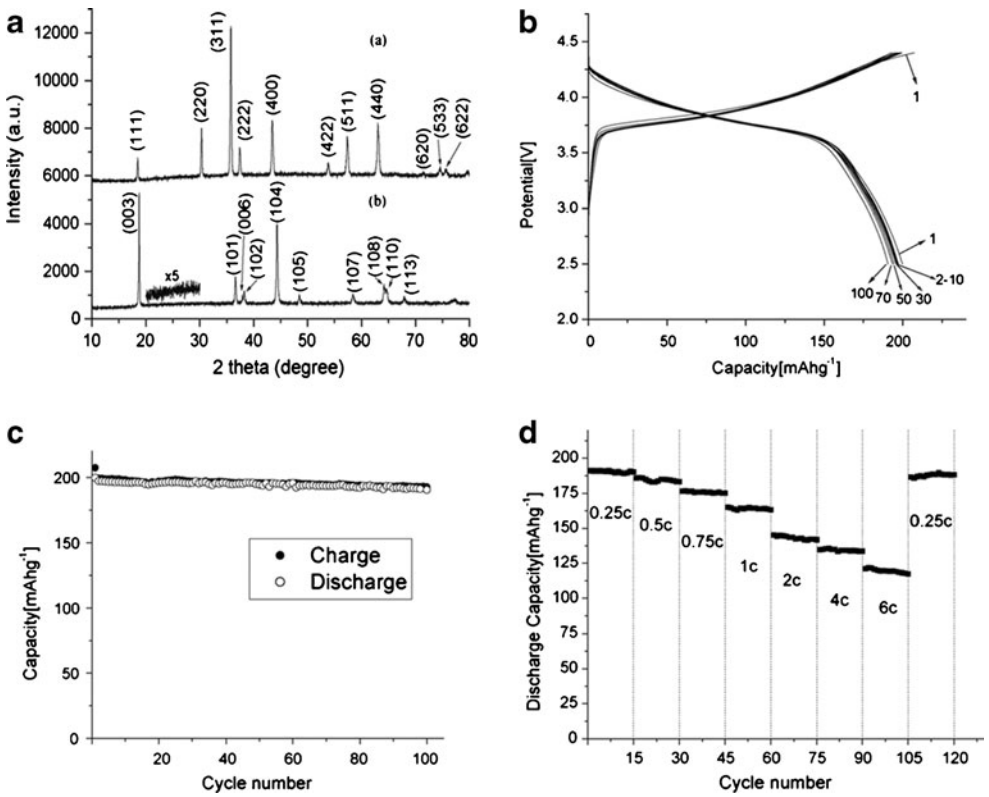

Fig. 2 **a** XRD patterns of precursor $Ni_{1.5}Mn_{1.5}O_4$ (*a*) and (*b*) $LiNi_{0.5}Mn_{0.5}O_2$; the *inset* in pattern (*b*) is magnified by ×5. **b** Galvanostatic cycles for a battery operated in the voltage from 2.5 to 4.4 V at a rate of 21.7 $mA\,g^{-1}$. **c** Charge and discharge capacities as a function of cycle number. **d** Discharge capacity at different current with cycle number (copyright 2008, Elsevier [42])

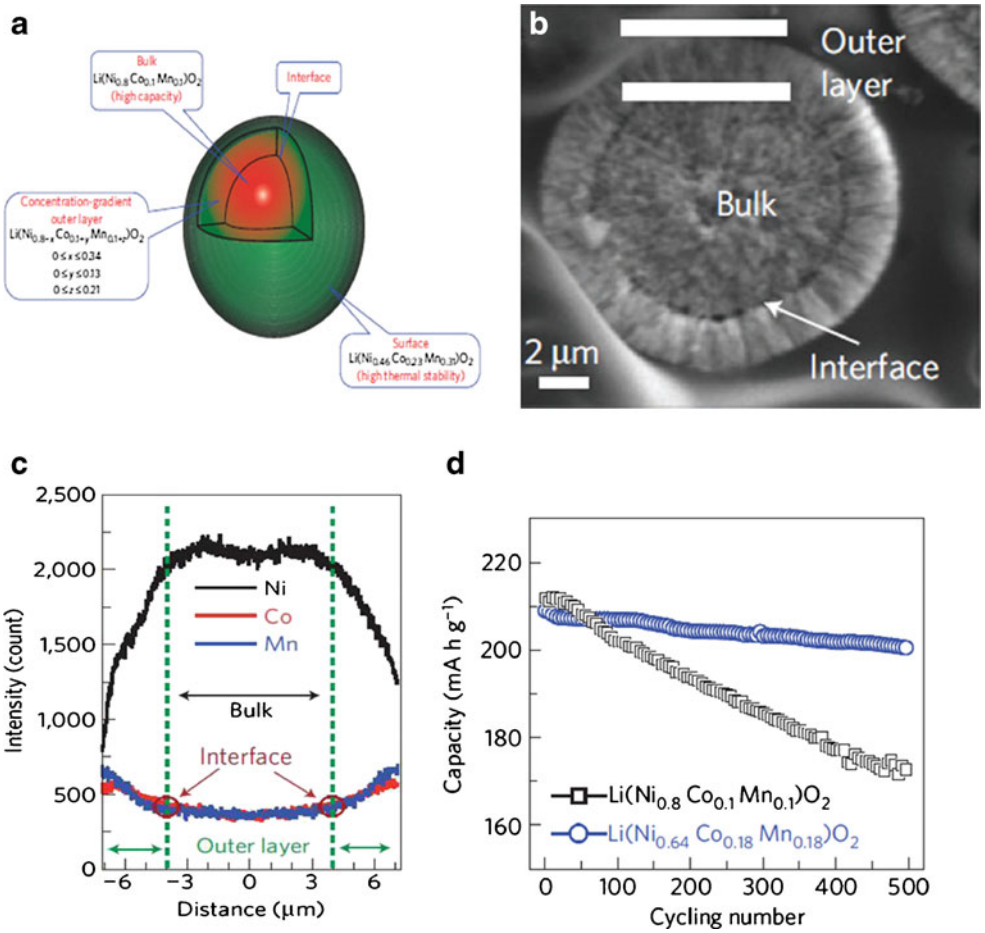

Fig. 3 **a** Schematic diagram of cathode electrode particle with Ni-rich core surrounded by concentration-gradient outer layer. **b** SEM of the core–shell structure $Li[Ni_{0.64}Co_{0.18}Mn_{0.18}]O_2$. **c** EPMA result of the core–shell structure $Li[Ni_{0.64}Co_{0.18}Mn_{0.18}]O_2$. **d** Cycling performance of laminated-type lithium-ion batteries concentration-gradient material as the cathode (copyright 2009, Nature [50])

concentrations remained nearly constant from the center to the interface. Between the interface and the surface of the particle, the Ni concentration decreased rapidly, whereas the Mn and Co concentrations increased gradually. Figure 3d shows the capacity retention of the $Li[Ni_{0.8}Co_{0.1}Mn_{0.1}]O_2$ and the core–shell material using an Al-pouch full cell with graphite as the anode. After 500 cycles, the concentration-gradient material showed higher capacity of over 96.5 % of its initial capacity, whereas the $Li[Ni_{0.8}Co_{0.1}Mn_{0.1}]O_2$ retained only 80.4 %. They contributed the higher retention to the core–shell structure because the increasing Mn concentration in the outer layer can limit the reactivity of the Ni ions with the electrolyte. The nickel-rich layered oxide satisfies high energy and power requirement for the P-HEVs, while the manganese ion provides outstanding cycle and safety in the outer layer. The profiles of differential scanning calorimetry indicate that the onset temperature of the exothermic reaction occurred at approximately 180 °C for $Li_{1-\delta}[Ni_{0.8}Co_{0.1}Mn_{0.1}]O_2$ whereas 270 °C for the concentration-gradient material. Therefore, compared with $Li_{1-\delta}[Ni_{0.8}Co_{0.1}Mn_{0.1}]O_2$, the reaction with the electrolyte was delayed by approximately 90 °C, owing to the high stability of the outer surface Mn-rich composition in core–shell structural material.

Effect of coating

Modification by coating is an important method to improve the electrochemical performance by means of modifying the surface chemistry or providing protection layer to minimize the direct contact of the active material with the electrolyte. The coating materials, the coating layers in other words, are able to suppress phase transition, increase the ionic or electronic conductivity, improve the structure stability, reduce transition metal dissolution, act as a HF scavenger to reduce the electrolyte acidity, and so on [51–58]. In addition, electrode resistance, side reactions, and heat generation during cycling are cut down, leading to a remarkable improvement in cycle life, rate capability, reversible capacity, coulomb efficiency, overcharge tolerance, and so forth [59–63].

The coating materials investigated in lithium nickel manganese oxides include metal oxides, e.g., ZnO [64], TiO_2 [65, 66], ZrO [67–69], Al_2O_3 [70–72], and MgO [73]; metal phosphate, e.g., $Zn_3(PO_4)_2$ or $Mg_3(PO_4)_2$ [74], $AlPO_4$ [75–77]; metal fluoride, e.g., AlF_3 [78–82]; various carbon [72, 83–88]; and other compounds [89–91]. The olivine $LiFePO_4$ can be added to coat the layered structure

materials such as $LiCoO_2$ [92, 93], $Li(Li_{0.17}Mn_{0.58}Ni_{0.25})O_2$ [93], and $LiNi_{0.5}Mn_{0.3}Co_{0.2}O_2$ [94] to improve capacity retention during cycling and performance at high discharge current.

Sun et al. investigated the proactive AlF_3 on the surface of various active materials [78–80, 95–97] and found that the capacity, capacity retention, and rate capability of these cathode electrodes in cell tests were improved because the interface between the cathode electrode and electrolyte was stabilized primarily. They speculated that the thin insulting AlF_3 coating suppressed the exothermic reaction with the liquid electrolyte [78, 95–97]. To further understand the detailed chemistry of the AlF_3 coating on the active materials, they studied the thermal behavior of the AlF_3-coated $Li[Ni_{1/3}Co_{1/3}Mn_{1/3}]O_2$ [98]. As shown in Fig. 4a, the AlF_3-coated $Li_{0.35}[Ni_{1/3}Co_{1/3}Mn_{1/3}]O_2$ still maintained the structure of $Li[Ni_{1/3}Co_{1/3}Mn_{1/3}]O_2$ with R-3m space group and presented a clear peak separation of the (108) and (110) doublets. The AlF_3-coated $Li[Ni_{1/3}Co_{1/3}Mn_{1/3}]O_2$ was covered with a layer of 10 nm thickness, and after the Li^+ extraction, the original surface was well preserved with the AlF_3 coating layer (Fig. 4b), indicating the excellent preservation of the original particle morphology. Compared with the uncoated $Li_{0.35}[Ni_{1/3}Co_{1/3}Mn_{1/3}]O_2$, the oxygen release occurs more slowly, and the amount was smaller for the AlF_3-coated materials as shown in Fig. 4c [99]. They also studied the thermal behavior in the presence of electrolyte by the DSC data for the chemically delithiated uncoated and AlF_3-coated $Li_{0.35}[Ni_{1/3}Co_{1/3}Mn_{1/3}]O_2$. From Fig. 4d, it is confirmed that the major thermal event occurred at a higher temperature, and the generated heat for exothermic reactions was smaller for the AlF_3-coated $Li_{0.35}[Ni_{1/3}Co_{1/3}Mn_{1/3}]O_2$. Therefore, the presence of AlF_3 coating on the surface of the delithiated $Li_{0.35}[Ni_{1/3}Co_{1/3}Mn_{1/3}]O_2$ is responsible for the improved thermal properties.

Carbon coating plays a more and more important role in new generation cathode materials due to the multifunctional advantages from the unique chemical and physical properties of carbon. When used as the coating material, it easily forms a thin film layer on the surface of the active materials, as shown in Fig. 5a [100]. The carbon can choose the structure of deposit in the form of amorphous carbon or nanosized graphite crystallite as illuminated in Fig. 5b, which allows the film to adjust the surface roughness and the curvature of the active particles [101]. The interspaces between disoriented nanocrystallite can ensure the ionic transport from the electrolytic medium to the core active particles by the diffusion of Li^+ throughout the micropores of the coating layer. The efficient electronic conductivity is because of that the sp^2 bonding prefers a layer-to-layer assembly of hexagonal atom planes, as shown in Fig. 5c. Compared with carbon coating, the metal oxide coating layer, composed of nanoparticles, is difficult to form a uniform thin layer due to the self-agglomeration and poor

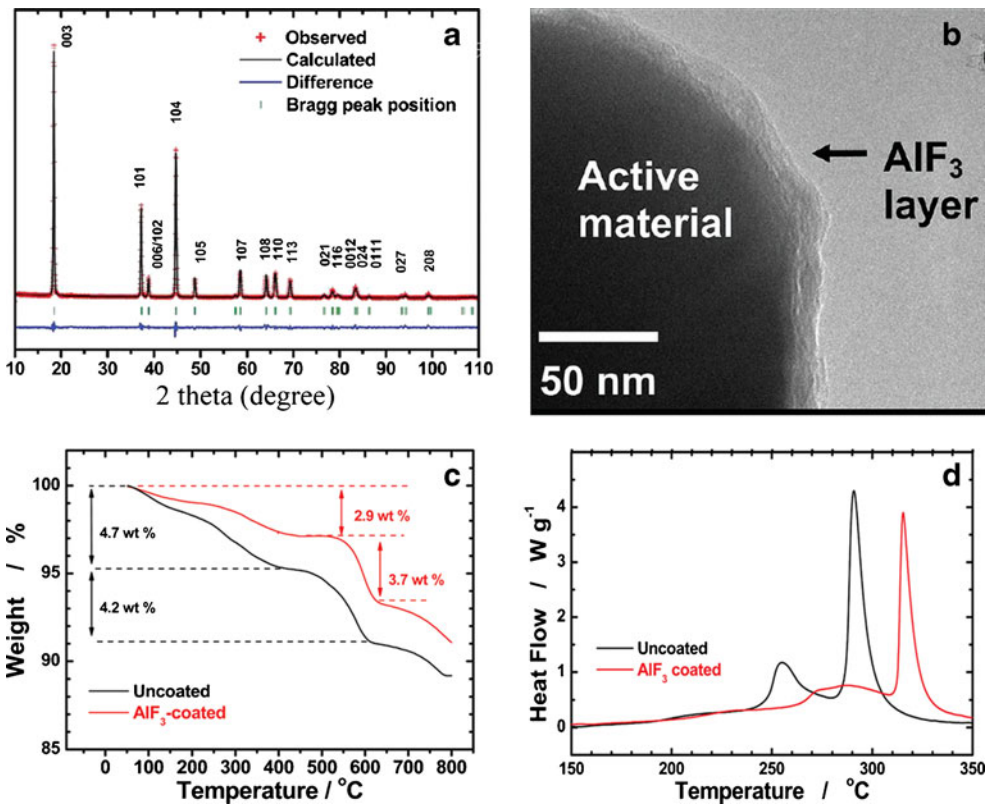

Fig. 4 **a** Rietveld refinement patterns of XRD data for the chemically delithiated AlF_3-coated $Li_{0.35}[Ni_{1/3}Co_{1/3}Mn_{1/3}]O_2$ and (**b**) corresponding TEM bright-field image. **c** TGA curves and (**d**) DSC curves of the chemically delithiated uncoated $Li_{0.35}[Ni_{1/3}Co_{1/3}Mn_{1/3}]O_2$ and AlF_3-coated $Li_{0.35}[Ni_{1/3}Co_{1/3}Mn_{1/3}]O_2$ (copyright 2010, ACS [98])

flexibility to geometry, as illustrated in Fig. 5d. Goodenough et al. investigated the influence of carbon coating on the performance of the $LiNi_{0.5}Mn_{0.5}O_2$ cathode and found that carbon coating suppressed the capacity fade by increasing the electronic conductivity and reducing cell polarization, and increased the discharge capacities at relatively high current densities [102]. Liu et al. successfully applied carbon coating on the layered $Li[Li_{0.2}Mn_{0.54}Ni_{0.13}Co_{0.13}]O_2$ by thermal evaporation of high purity graphite rod [103]. Comparing the SEM images of the $Li[Li_{0.2}Mn_{0.54}Ni_{0.13}Co_{0.13}]O_2$ particles on the electrode film before and after coating, they found it becomes coarse after carbon coating, as shown in Fig. 6a. The carbon-mapping image confirmed the carbon coating layer on the cathode material surface, and the coating was uniform. The carbon-coated electrode showed higher rate capability than the bare electrode observed from Fig. 6b, the discharge profile at various C rate of the electrode before and after coating with carbon. Compared with the discharge capacity at a high rate 2C of the electrodes in 30 cycles before and after coating, the carbon-coated sample exhibited much better capacity retention. The improved capacity retention is due to the protection of the electrode surface by the carbon coating from electrolyte and the suppression of the formation of thick SEI layer, as shown in Fig. 6d. In addition, the surface electronic conductivities of bare and carbon-coated $Li[Li_{0.2}Mn_{0.54}Ni_{0.13}Co_{0.13}]O_2$ electrodes were found to be 0.696 and 0.975 Scm^{-1}, respectively, indicating a 40 % enhancement by coating with carbon.

Modified by doping

The performance of layered Li-Ni-Mn-O cathode materials can be improved by doping, through either affecting the microstructure or morphology or stabilizing the layered crystal structure. The doping additions include metal, e.g., iron [104], Cr [105–107], Zn [108], Ti [104, 109], Zr [110], Al [104, 107, 111–117], Mg [107, 118, 119], and fluorine [120, 121].

Among the various doping additions, cobalt was found to be the most effective addition to the $LiNi_{0.5}Mn_{0.5}O_2$. The electrochemical performance of $LiNi_{0.5-x}Mn_{0.5-x}Co_{2x}O_2$ can be improve by doping a small amount of cobalt, and the more amount of cobalt, the better the rate capacity of $LiN_{i0.5-x}Mn_{0.5-x}Co_{2x}O_2$ when the value of x is in the range of 0–0.5. As early as 2001, the electrochemical performance of $LiCo_{1/3}Ni_{1/3}Mn_{1/3}$ was already reported by Ohzuku et al. [122]. Afterwards, the importance of the series of Li-Ni-Mn-Co-O materials is more recognized, as the presence of Co ions can help to reduce the amount of defect Ni in Li layers [123]. $LiCo_{1/3}Ni_{1/3}Mn_{1/3}O_2$ delivers similar reversible capacity, similar in voltage profile shape, extended operation voltage window with $LiNi_{0.5}Mn_{0.5}O_2$. A great deal of researches has been made to investigate the electrochemical performance of the material. Ohzuku et al. investigated the electrochemical behavior of $LiCo_{1/3}Ni_{1/3}Mn_{1/3}O_2$ in lithium batteries at elevated temperatures [124]. They found that $LiCo_{1/3}Ni_{1/3}Mn_{1/3}O_2$ was capable to deliver 160 $mAhg^{-1}$ of capacity even at 20C corresponding to 4,000 mAg^{-1} at 55 °C, as shown in Fig. 7a. Figure 7b showed the discharge

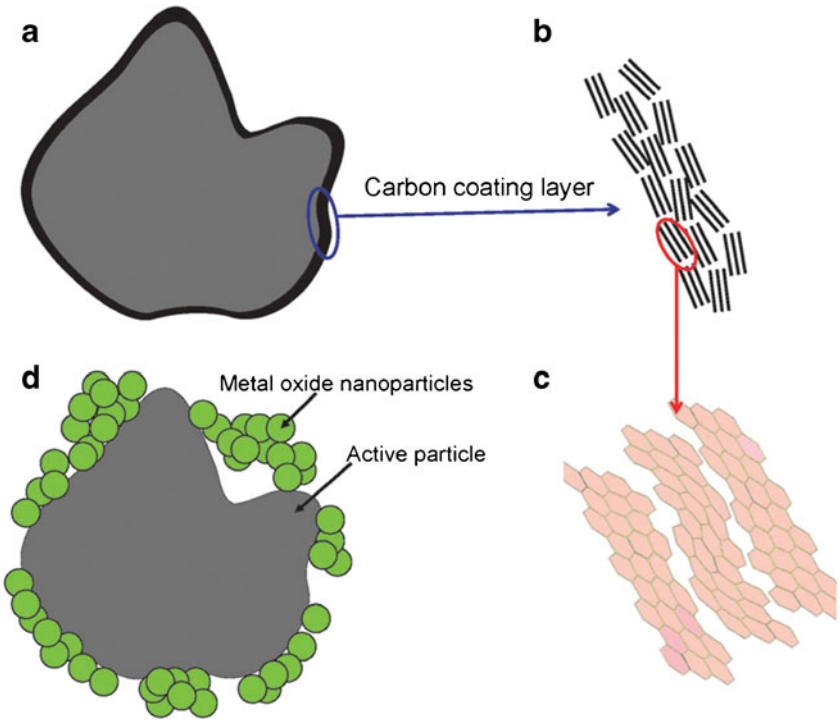

Fig. 5 Schematic illustrations showing different adaptability of the carbon coating (**a**) and metal oxide coating (**d**) to the geometry of the substrate material. **b**, **c** More details of the carbon coating layer (copyright 2012, RCS [100])

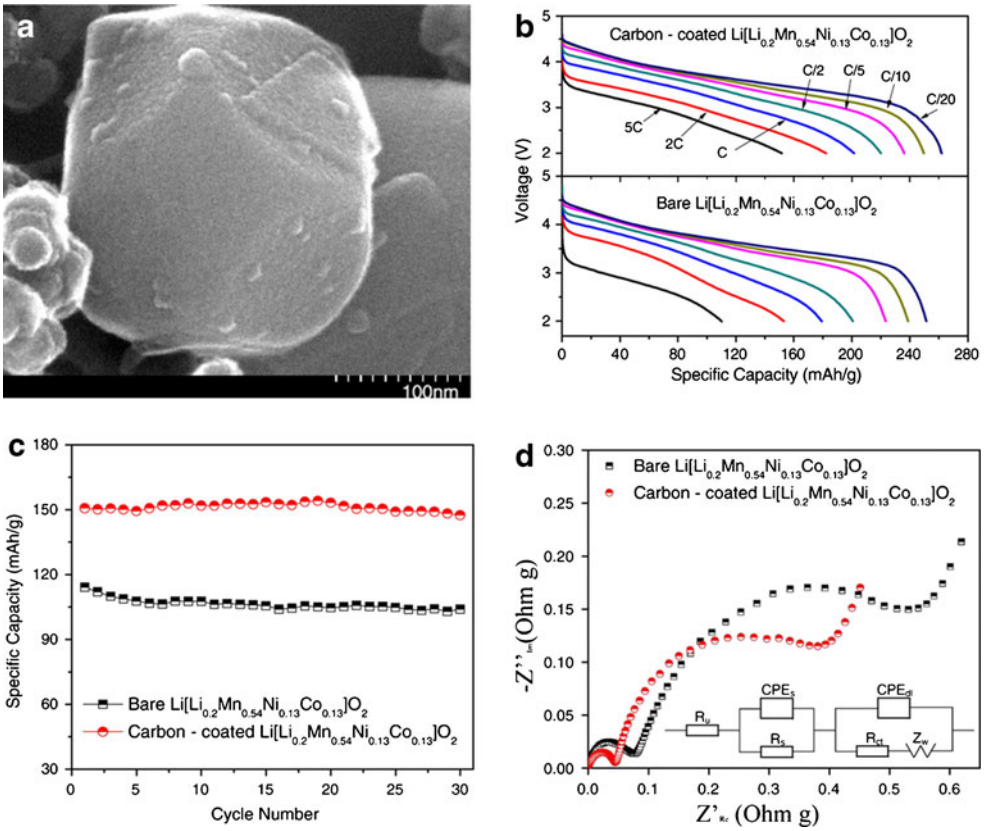

Fig. 6 **a** SEM image of the carbon-coated $Li[Li_{0.2}Mn_{0.54}Ni_{0.13}Co_{0.13}]O_2$ particle, (**b**) discharge profiles at various C rates, (**c**) cycling performance, and (**d**) Nyquist plots of bare and carbon-coated $Li[Li_{0.2}Mn_{0.54}Ni_{0.13}Co_{0.13}]O_2$ electrodes (copyright 2010, Elsevier [103])

capacity as a function of cycle number of a $Li[Li_{1/3}Ti_{5/3}]/LiCo_{1/3}Ni_{1/3}Mn_{1/3}O_2$ cell operated at elevated temperatures in voltages of 1.0–3.05 V, indicating that $LiCo_{1/3}Ni_{1/3}Mn_{1/3}O_2$ was the most promising cathode electrode material for advanced Li-ion batteries. Similarly, Bruce et al. synthesized macroporous $LiCo_{1/3}Ni_{1/3}Mn_{1/3}O_2$ composed of individual particles of narrow size distribution [125]. The charge/discharge curves that obtained cells containing macroporous $LiCo_{1/3}Ni_{1/3}Mn_{1/3}O_2$ were presented in Fig. 7c. The first charge corresponded to a capacity of 234 $mAhg^{-1}$, with the subsequent discharge yielding 209 $mAhg^{-1}$, and a capacity of 190 $mAhg^{-1}$ was obtained on cycle 220 representing capacity retention of 99.99 % per cycle from cycle 20 to cycle 220. Voltage for discharging from 4.6 to 2.5 V at increasing rate from 20 to 4,000 mAg^{-1} was shown in Fig. 7d. Capacity on discharge was reduced to 84 % on increasing the discharge rate from 1 to 20C, demonstrating that the macroporous material can sustain excellent charge and discharge rates. The reduced amount of Co can be used to achieve the same benefit reported by Li et al. [126]. Comparative study of the capacity and rate capability of $LiNi_yMn_yCo_{1-2y}O_2$ was investigated. Figure 8a shows the first cycle of $LiNi_yMn_yCo_{1-2y}O_2$ and found that the $LiCo_{1/3}Ni_{1/3}Mn_{1/3}$ material had a slightly lower effective capacity, indicating the involvement of Co redox process pushing the voltage higher. The cycling performance of the $LiNi_yMn_yCo_{1-2y}O_2$ is shown in Fig. 8b, indicating that the $LiNi_{0.4}Mn_{0.4}Co_{0.2}O_2$ material showed a slightly higher discharge capacity than the other composition at low rate. According to the discharge behavior of the $LiNi_yMn_yCo_{1-2y}O_2$ as shown in Fig. 8c, the higher the cobalt content, the better the rate performance. Therefore, taking electrochemical performance and cost, the $LiNi_{0.4}Mn_{0.4}Co_{0.2}O_2$ composition might be expected to achieve higher rates.

Manufactured to lithium-rich materials

Lithium-rich cathode materials can be considered the solid solution of monoclinic (C2/m) Li_2MnO_3, with layered structure materials including $LiNi_{0.8}Co_{0.15}Zr_{0.05}O_2$ [127], $LiNi_{0.5}Mn_{0.5}O_2$ [128], $LiNi_{1/3}Mn_{1/3}Co_{1/3}O_2$ [129–133], and other Li(Ni, Mn, Co)O_2 compositions [128, 133–137], which act as a lithium reserve and improve capacity retention during cycling together.

Yang et al. prepared a series of cathode materials $xLi[Li_{1/3}Mn_{2/3}]O_2$ $(1-x)Li[Ni_{1/3}Mn_{1/3}Co_{1/3}]O_2$ $(0 \le x \le 0.9)$ by combination of co-precipitation and solid-state calcination method [131]. The materials were characterized by X-ray diffraction (XRD), as shown in Fig. 9a. All the patterns can be indexed to a single phase of the α-$NaFeO_2$ type with space group R-3m except for the small peaks at $2\theta = 20.85°$, 21.79°, and 24.31° which can be indexed to C2/m space group. The (108)/(110) peaks splitting, which is considered as an evidence for the degree of ordering layered structure, was pointed out with emphasis. The larger the x, the larger

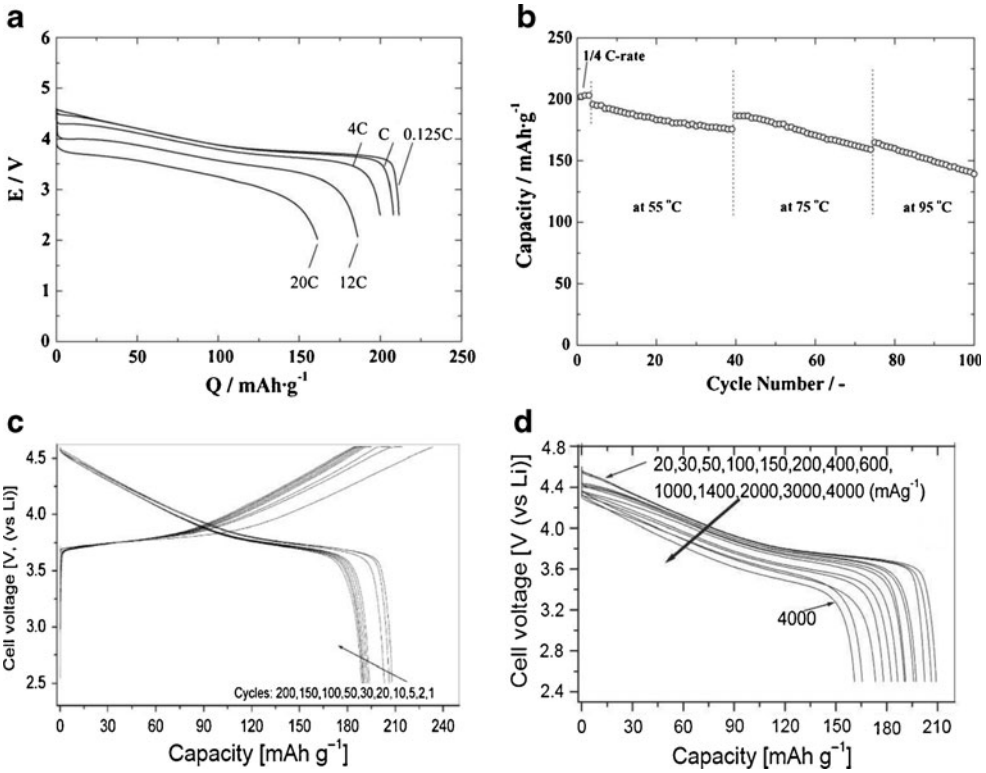

Fig. 7 **a** Rate capability tests on a Li/$LiCo_{1/3}Ni_{1/3}Mn_{1/3}O_2$ cell. **b** Cycling performance of a Li[$Li_{1/3}Ti_{5/3}$]/$LiCo_{1/3}Ni_{1/3}Mn_{1/3}O_2$ cell operated at elevated temperatures (copyright 2005, Elsevier [124]). **c** Voltage versus capacity profiles for Li($Ni_{1/3}Co_{1/3}Mn_{1/3}$)O_2, and (**d**) rate performance at room temperature (copyright 2006, WILEY-VCH [125])

the peaks splitting, as indicated in Fig. 9b. In addition, according to the configurations of Li[$Ni_{1/3}Mn_{1/3}Co_{1/3}$]O_2 and Li[$Li_{1/3}Mn_{2/3}$]O_2, they assumed that the two figures alternate with the ratio of x:(1−x) in transition metal layer. The particles of 0.6Li[$Li_{1/3}Mn_{2/3}$]O_2 0.4Li[$Ni_{1/3}Mn_{1/3}Co_{1/3}$]O_2 were homogenously distributed with the particle size between 0.1 and 0.5 μm from the scanning electron micrograph, as shown in Fig. 9c. Figure 9d shows the cycling performances of the xLi[$Li_{1/3}Mn_{2/3}$]O_2 (1−x)Li[$Ni_{1/3}Mn_{1/3}Co_{1/3}$]O_2 electrode materials. As observed, the materials xLi[$Li_{1/3}Mn_{2/3}$]O_2 (1−x)Li[$Ni_{1/3}Mn_{1/3}Co_{1/3}$]O_2 delivered high specific capacity and good cycling performance. Especially, an initial discharge capacity of 250 $mAhg^{-1}$ was obtained for sample 0.6Li[$Li_{1/3}Mn_{2/3}$]O_2 0.4Li[$Ni_{1/3}Mn_{1/3}Co_{1/3}$]O_2, which is an excellent constant with the theoretical capacity from fully delithiated 0.6Li[$Li_{1/3}Mn_{2/3}$]O_2 0.4Li[$Ni_{1/3}Mn_{1/3}Co_{1/3}$]O_2 electrode, 251 $mAhg^{-1}$. In this kind of materials, it is believed that the Li[$Ni_{1/3}Mn_{1/3}Co_{1/3}$]O_2 offer only 50–60 % of their full capacity (140–170 $mAhg^{-1}$), and stabilized Li_2MnO_3 cathode offer at best between 120 $mAhg^{-1}$ of capacity [138]. Moreover, an anomalously high capacity in excess of the theoretical value, typically 280–300 $mAhg^{-1}$, can be obtained [139]. In most cases, the capacity declines during the early cycles to the theoretical or lower values [140]. In such an anomalously high capacity in condition that the lithium completely delithiated, how does the electrode structure stabilize? Thackeray et al. made system research on the structure of Li_2MnO_3-$LiMO_2$ and considered that the materials are characterized by Mn and M cation disorder between the Li_2MnO_3 and $LiMnO_2$ compounds, as shown in Fig. 10 [139]. Comparing the material structure before and after lithium delithiated, the Li_2MnO_3 component plays a vital function in the electrochemical operation of $x$$Li_2MnO_3$-(1−$x$)$LiMO_2$ electrodes: Firstly, by extracting Li_2O in a controlled manner, the Li_2MnO_3 component is activated to form MnO_2 component within a charged electrode structure, making these materials extremely versatile for tailoring and optimizing their composition, structure, and electrochemical properties; secondly, Li_2MnO_3 acts as a reservoir for excess lithium diffusing from the transitional metal layers into adjacent lithium-depleted layers during charge to stabilize the material structure, consequently, the access of high practical capacities obtained; lastly, Li_2MnO_3 can facilitate the Li^+ transport through the structure as solid electrolyte constituents.

Recently, Komaba et al. studied the reaction mechanism of 0.5Li_2MnO_3 0.5Li[$Ni_{1/3}Mn_{1/3}Co_{1/3}$]O_2 in detail before and after charging across a voltage plateau at 4.5 V vs. Li/Li^+ [132]. On the basis of their analysis, it is proposed that high capacity of the Li excess manganese layered oxides after the first charge to the high voltage is divided into two mechanisms, as summarized in Fig. 11: one is the activated manganese redox reaction (Mn^{3+}/Mn^{4+}), and another is the oxygen reduction at the electrode surface. When charged to 4.8 V beyond the high voltage plateau, lithium and oxide ions are simultaneously extracted from the oxide particles. This process is accompanied by the cation rearrangement

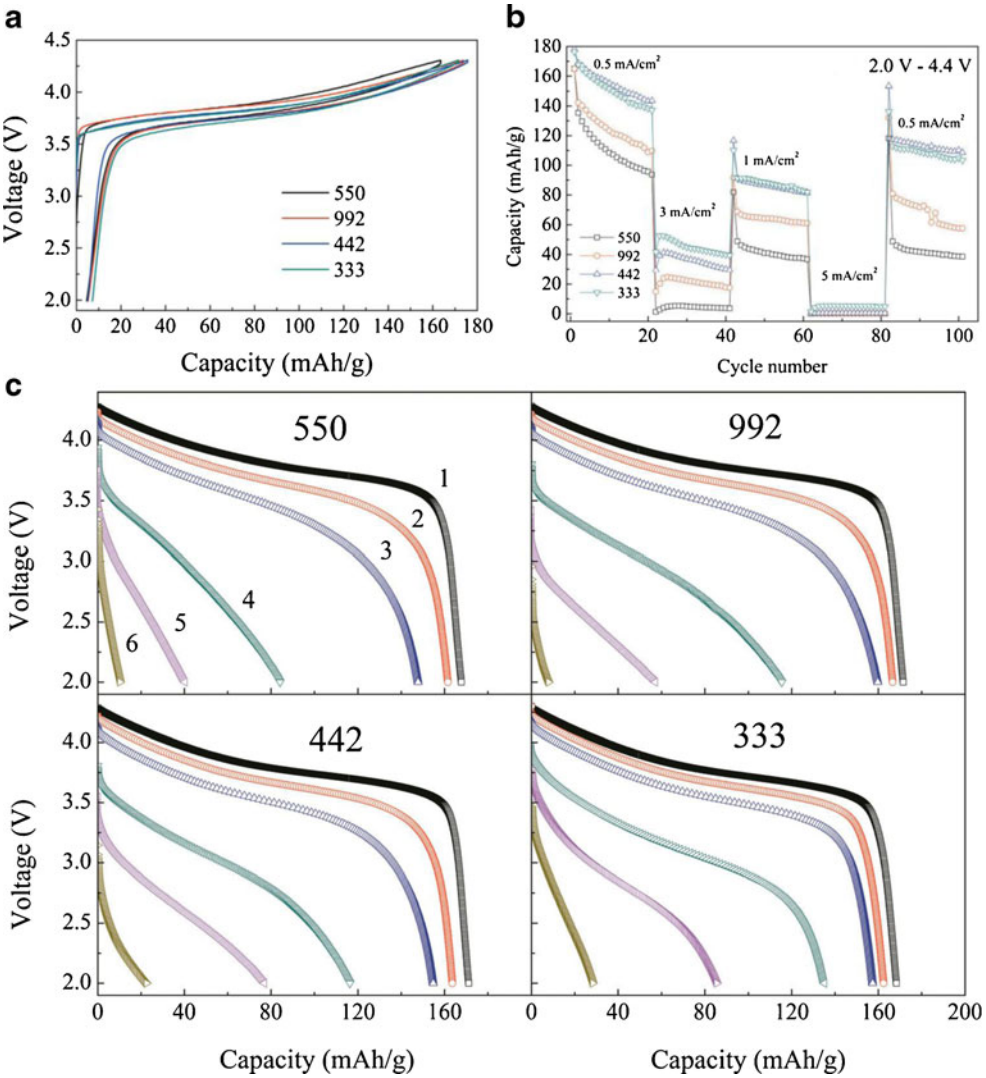

Fig. 8 **a** The first cycle of $LiNi_yMn_yCo_{1-2y}O_2$. **b** The cycling performance of $LiNi_yMn_yCo_{1-2y}O_2$ between 2.0 and 4.4 V. **c** The discharge curves at different current densities for $LiNi_yMn_yCo_{1-2y}O_2$; *1–6* indicate 0.1, 0.5, 1, 3, 5, and 8 mA cm^{-2}, respectively. For y=0.5, 550; y=0.45, 992; y=0.4, 442; and y=0.33, 333 (copyright 2011, the Electrochemical Society [126])

process including the nickel migration from the metal layer to lithium layer. In the meantime, the tetravalent manganese ions in the pristine sample are partially oxidized to the trivalent state in discharge process. For the latter mechanism, oxygen is electrochemically reduced at the electrode surface in the discharge process below 3 V, which resulted in the deposition on the electrode surface, specifically on carbon and oxides. The electrochemically active oxygen is consumed by the formation of Li_2CO_3, and then the reversible capacity related to the surface redox reaction declines.

Nanostructured material

The electrode reaction occurs at the surface and requires transport of ions into the electrode material. Therefore, the smaller the particles, the higher the surface area and the shorter the diffusion distance they can provide. In addition, the electron transport within the particles is enhanced by nanometer-sized particles [141], and the thermodynamics of the reaction can be modified [142]. However, nanoparticles have some disadvantages, such as diffusion of ions in the electrolyte to the particles surface and reduced volumetric energy density [143], which may bring rate limiting. In spite of these shortages, the nanostructured materials are a key for better performance in Li-ion batteries [144].

In 2004, Hong et al. prepared nanocrystalline $Li[Ni_{0.20}Li_{0.20}Mn_{0.60}]O_2$ by simple combustion method [145]. The micrometer particles consisted of aggregates of small primary particles distributed in the range of 80–200 nm, as shown in Fig. 12a. The initial discharge capacity was about 288 mAh g^{-1} at the current rate of 20 mA g^{-1}. In addition, at 400 mA g^{-1}, a reversible discharge capacity of 200 mAh g^{-1} was still observed as illustrated in Fig. 12b. However, the discharge capacity fade at low currents was more than at high currents, as observed in Fig. 12c. Interestingly, there was a significant capacity loss of

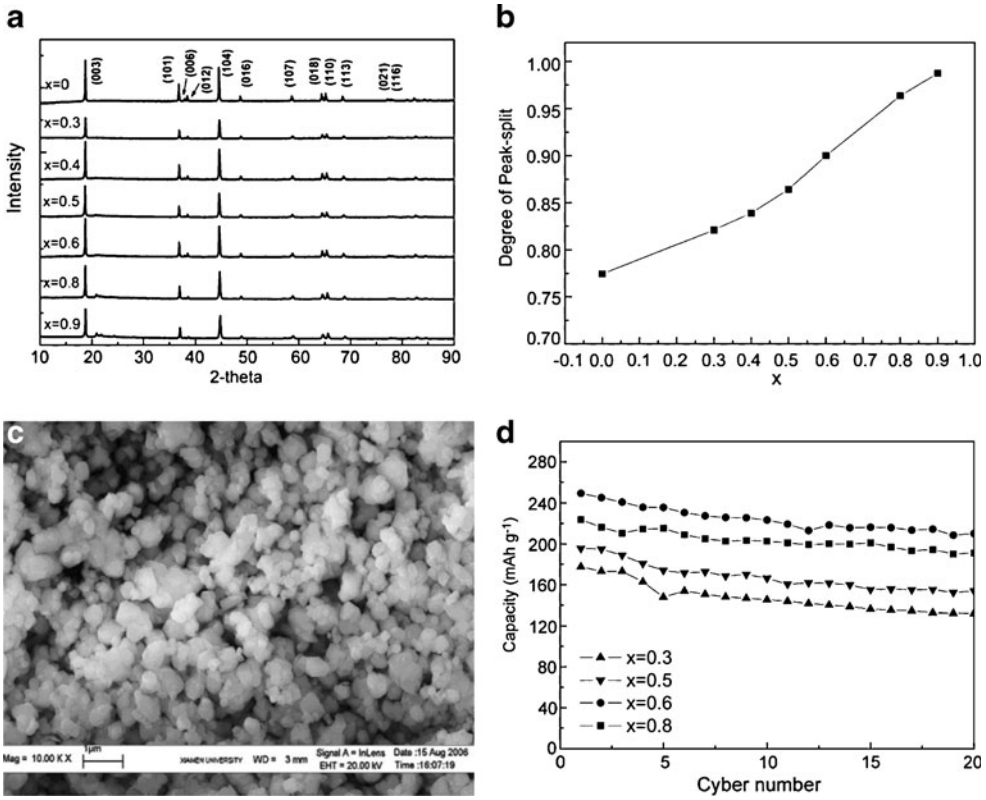

Fig. 9 **a** XRD patterns of $x\text{Li}[\text{Li}_{1/3}\text{Mn}_{2/3}]\text{O}_2$ $(1-x)\text{Li}[\text{Ni}_{1/3}\text{Mn}_{1/3}\text{Co}_{1/3}]\text{O}_2$ $(0\le x\le 0.9)$. **b** Peak splitting of (108) and (110) vs. x. **c** SEM image of $0.6\text{Li}[\text{Li}_{1/3}\text{Mn}_{2/3}]\text{O}_2$ $0.4\text{Li}[\text{Ni}_{1/3}\text{Mn}_{1/3}\text{Co}_{1/3}]\text{O}_2$ material. **d** Cycling performance of the Li/$x\text{Li}[\text{Li}_{1/3}\text{Mn}_{2/3}]\text{O}_2$ $(1-x)\text{Li}[\text{Ni}_{1/3}\text{Mn}_{1/3}\text{Co}_{1/3}]\text{O}_2$ $(0\le x\le 0.9)$ cells (copyright 2008, Elsevier [131])

several tens of cycles; thereafter, the capacity of the cell steadily increased and stabilized on cycling. Figure 12d showed the discharge capacity obtained at specific currents varying from 20 to 900 mA g^{-1}, which showed that an excellent reversible capacity was retained at specific current as high as 800 mA g^{-1} due to the nanocrystalline particle size of 80–200 nm. Thereafter, Cho et al. prepared $\text{Li}[\text{Ni}_{0.41}\text{Li}_{0.08}\text{Mn}_{0.51}]\text{O}_2$ consisted of stacked nanoplates with a plate thickness of approximately 7 nm (Fig. 13a, b) [146]. The electrochemical cycling results showed a maximum reversible capacity of 200 mAh g^{-1} between 2 and 4.8 V with little capacity loss after 30 cycles, as illustrated in Fig. 13c. Furthermore, in contrast to the sample prepared by solid-state method, the capacity loss of the nanoplates is much smaller at higher rates, as can be seen in Fig. 13d. Next, they synthesized $\text{Li}[\text{Ni}_{0.25}\text{Li}_{0.15}\text{Mn}_{0.6}]\text{O}_2$ nanowires [147] with a diameter of about 30 nm, as shown in Fig. 14a–c. The nanowires exhibited a

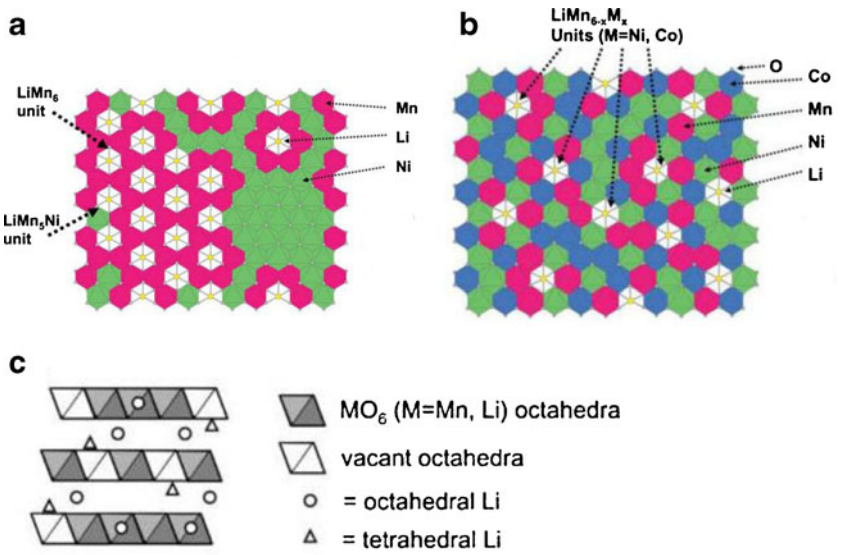

Fig. 10 Schematic structural illustrations corresponding to (**a**) Li_2MnO_3-$\text{LiNi}_{0.5}\text{Mn}_{0.5}\text{O}_2$, (**b**) Li_2MnO_3-$\text{LiNi}_{0.333}\text{Mn}_{0.333}\text{Co}_{0.333}\text{O}_2$, and (**c**) a delithiated Li2MnO3-like region of xLi2MnO3 $(1-x)$LiMO2 electrode structure (M =Mn, Ni, and Co; copyright 2007, RSC [139])

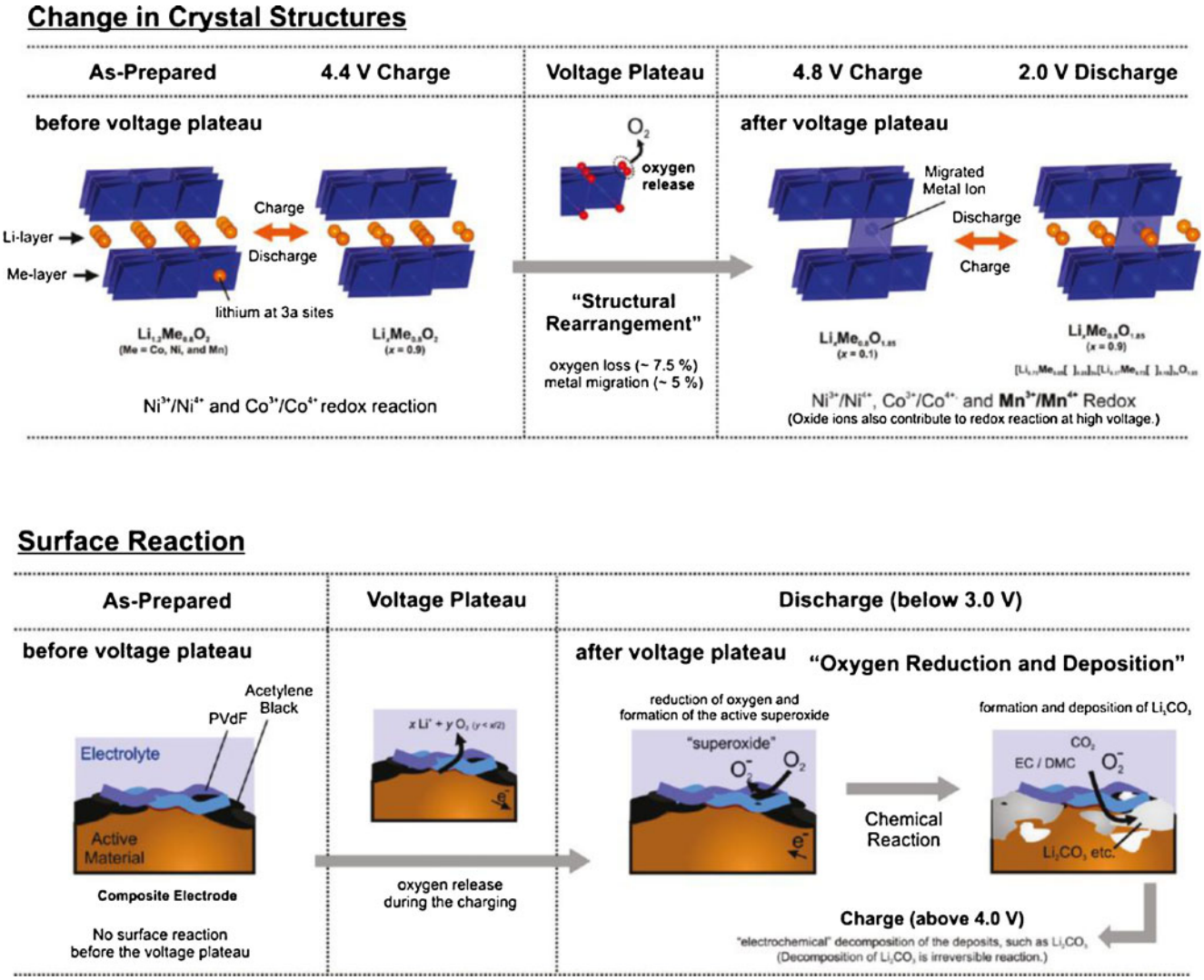

Fig. 11 Schemes of the proposed reaction mechanisms in the $0.5Li_2MnO_3$ $0.5Li[Ni_{1/3}Mn_{1/3}Co_{1/3}]O_2$ lithium-rich electrodes consisting of the active material, acetylene black, and PVdF (copyright 2011, ACS [132])

first discharge capacity of 311 $mAhg^{-1}$ at 120 mAg^{-1} (Fig. 14d). After 80 cycles, the capacity retention is 95 % with a discharge capacity of 294 $mAhg^{-1}$ (Fig. 14e). The rate capabilities of the nanowires were also far superior to those of their nanoplate counterpart, showing the discharge capacity of 256 $mAhg^{-1}$ at 7C rate (Fig. 14f). The nanowires showed a significantly improved capacity and rate capabilities compared to nanoparticles. Recently, $LiCo_{1/3}Mn_{1/3}Ni_{1/3}O_2$ hollow spheres with an average outer diameter of 300 nm and a wall thickness of about 50 nm are prepared [148]. They demonstrate excellent electrochemical performance, including high discharge capacity and rate capability. At a current rate of 0.2C (34 mAg^{-1}, 0.34 $mAcm^{-2}$), cathode materials constituted by the hollow spheres display a discharge capacity of 175.4 $mAhg^{-1}$. Even at a current rate of 10C (1,700 mAg^{-1}, 17 $mAcm^{-2}$), the discharge capacity also keeps at 91.5 $mAhg^{-1}$.

Prospect of layered Li-Ni-Mn-O cathode materials

Up to now, a lot of effort has been made to develop the structure and electrochemical performance of layered Li-Ni-Mn-O cathode materials. However, there are still some challenges that remain in the structure and electrochemical mechanism of layered Li-Ni-Mn-O cathode materials. As can be seen from the above discussion, various modification methods, including coating, doping, synthesis method, lithium-rich materials, and nanostructured materials, are of benefit to the improvement of the electrochemical properties of the layered Li-Ni-Mn-O cathode materials. The comparison of the reviewed modification method in lithium half-cell can be expressed with a diagram, as indicated in Fig. 15. Except the lithium-rich materials xLi_2MnO_4 $(1-x)LiMO_2$, all other materials modified by coating, doping, and synthesis are restricted in their capacities in the range of theoretical

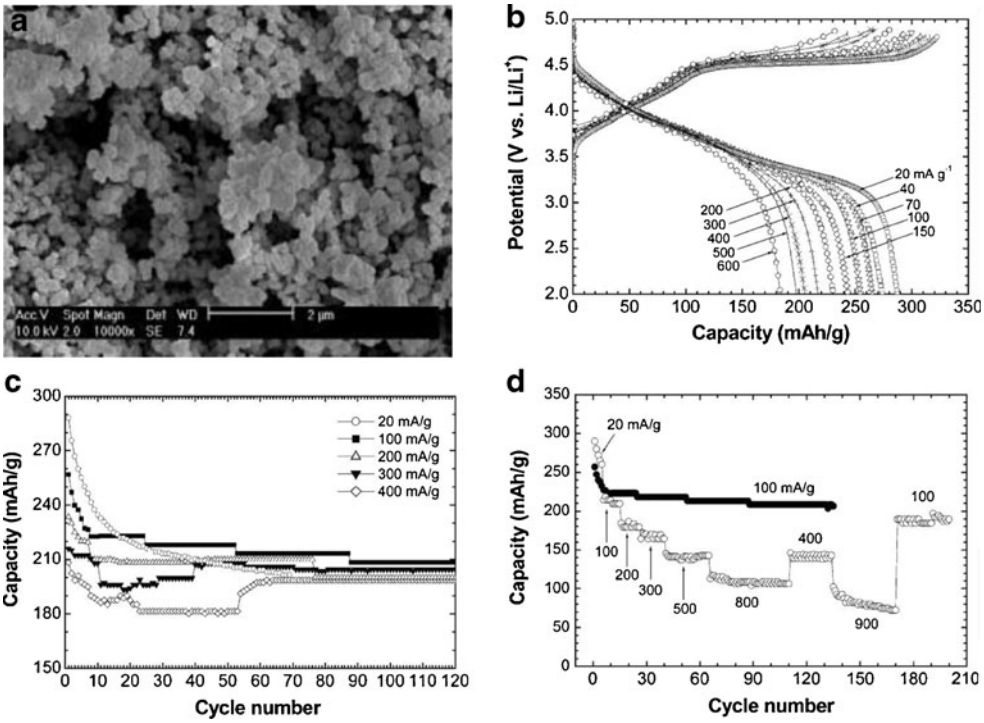

Fig. 12 **a** SEM photograph of $Li[Ni_{0.20}Li_{0.20}Mn_{0.60}]O_2$. **b** Initial charge/discharge curves. **c** Capacity retention vs. cycle number for the Li/$Li[Ni_{0.20}Li_{0.20}Mn_{0.60}]O_2$ cells cycled between 4.8 and 2.0 V at various specific currents. **d** Rate capability of $Li[Ni_{0.20}Li_{0.20}Mn_{0.60}]O_2$ observed in continuous cycling at specific currents varying from 20 to 900 mA g^{-1} (copyright 2004, RSC [145])

capacity. After modification, the layered lithium nickel manganese oxides cathode materials not only stabilize their structure in the process of charge and discharge but also ameliorate the electrochemical properties. What is more, the lithium-rich materials xLi_2MnO_4 (1 $-x$)$LiMO_2$ as cathode materials can obtain the practical capacities much higher than the theoretical capacities and can receive the rechargeable capacity of near the theoretical value. In addition, the core–shell structured Li-Ni-Mn-O materials also have the large rechargeable

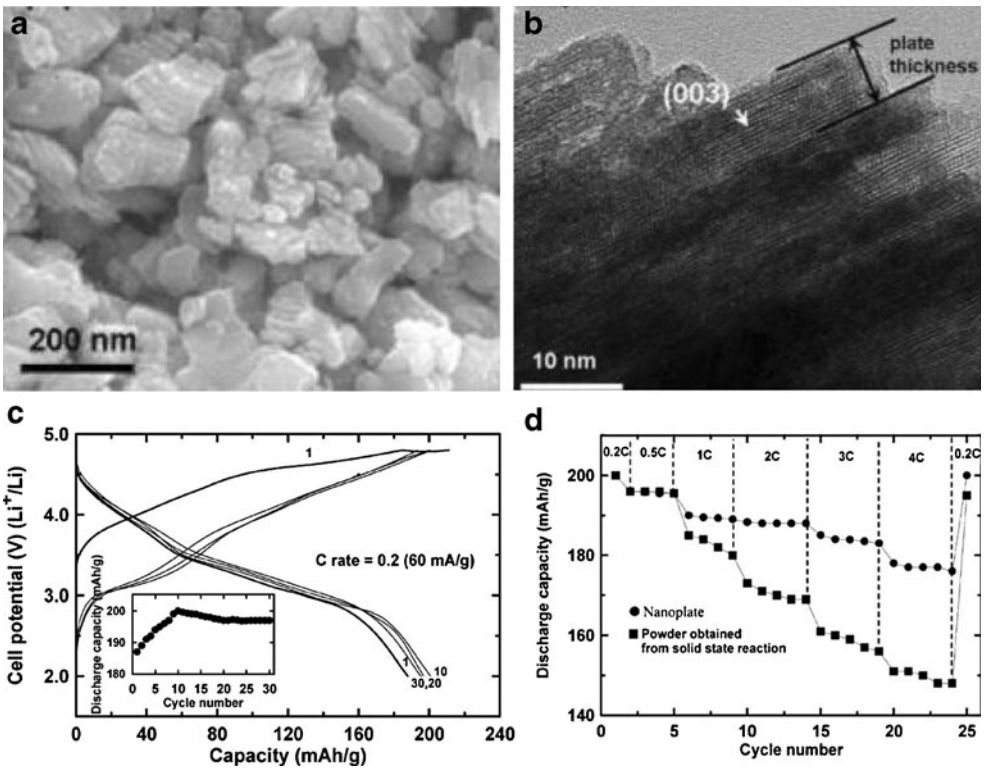

Fig. 13 **a** SEM and (**b**) TEM images of $Li[Ni_{0.41}Li_{0.08}Mn_{0.51}]O_2$. **c** Voltage profiles of the $Li[Ni_{0.41}Li_{0.08}Mn_{0.51}]O_2$ cathode after 1, 10, 20, and 30 cycles (*inset* is a plot of the discharge capacity as a function of the cycle number). **d** The rate capabilities of the nanoplates and powder prepared by solid-state method at 0.2, 0.5, 1, 2, 3, and 4C rates (copyright 2007, ACS [146])

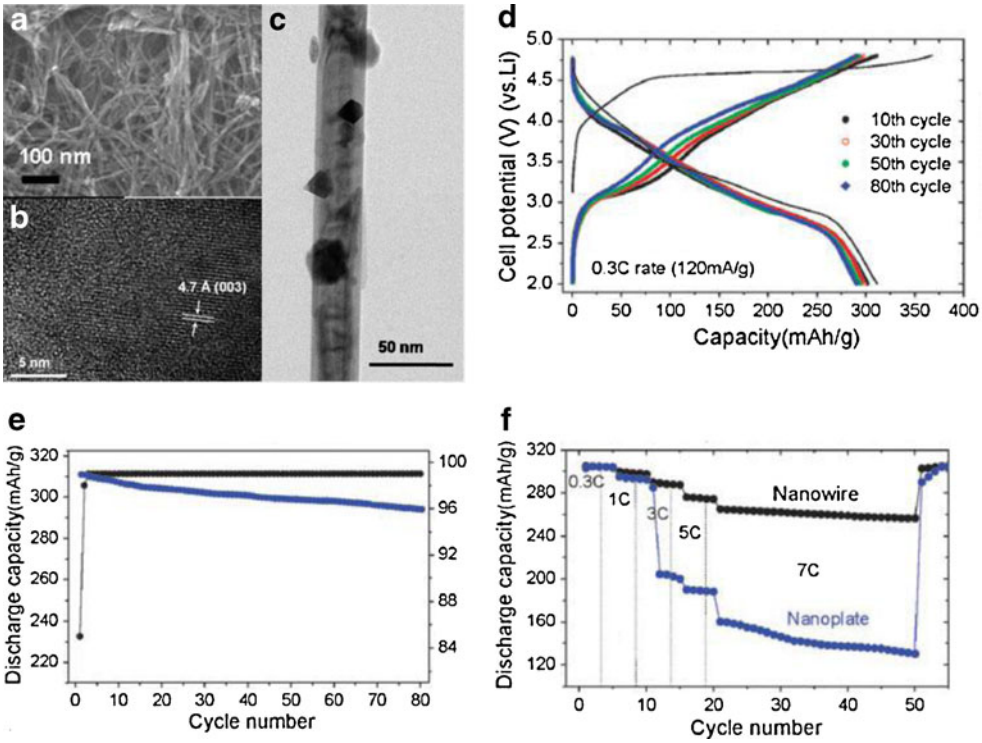

Fig. 14 **a** TEM image of the $Li[Ni_{0.25}Li_{0.15}Mn_{0.6}]O_2$ nanowires, and **b** and **c** expanded images of **a**. **d** Charge and discharge curves of the $Li[Ni_{0.25}Li_{0.15}Mn_{0.6}]O_2$ nanowires. **e** Plot of cycle life and coulombic efficiency of the nanowires as a function of the cycle number. **f** Rate capabilities of the nanowires and nanoparticles with the $Li[Ni_{0.25}Li_{0.15}Mn_{0.6}]O_2$ composition at different C rate (copyright 2009, RSC [147])

capacity and comparable high operating voltage. Therefore, the properties of the layered lithium nickel manganese oxides can be made better by the modification mentioned above.

However, the limitations exist when the Li-Ni-Mn-O materials are modified by one method individually. For the core–shell structured Li-Ni-Mn-O cathode materials, although it has thermal stability in highly delithiated state, it is not satisfactory about the less rechargeable capacity less than 210 $mAhg^{-1}$. In addition, for coating and doping materials, the rechargeable capacity is also difficult to break through the value. As for the lithium-rich materials xLi_2MnO_4 $(1-x)LiMO_2$, they have enormous potential and higher discharge capacity. However, Li_2O formed in the discharge process, which causes their initial irreversibility. In addition, at such a high voltage cut-off during charge, the stability of electrolyte can not be guaranteed. In spite of these shortcoming, lithium-rich materials xLi_2MnO_4 $(1-x)LiMO_2$ have taken lots of attention owing to the high capacity. The initial irreversibility can be solved by the preparation of xLi_2MnO_4 $(1-x)LiMO_2$ distributed in nanosize or core–shell structure with modification of coating or doping.

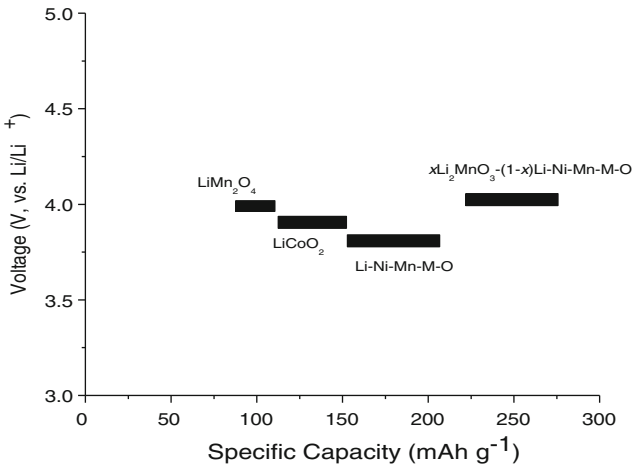

Fig. 15 Specific capacity and working potential of the cathode materials discussed in the review

Conclusions

In conclusion, the development of the lithium nickel manganese oxide cathode materials is reviewed. Lithium nickel manganese oxides are promising, inexpensive, and nontoxic in addition to having a high thermal stability, thus are attracting much attention as alternative cathode electrode materials to the commercial $LiCoO_2$ electrode. It is pointed out that the cycle performance and rate capability can be solved by the combination of lithium-rich materials xLi_2MnO_4 $(1-x)LiMO_2$ and nanosized material or core–shell structure with modification of coating and doping. However, much more ongoing effort should be made to develop new materials with enormous potential and high cycling capacity to catch up with the development of the anode materials.

Acknowledgment This work was supported by the doctor initial foundation of Baoji University of Arts and Sciences (ZK1052).

References

1. Tarascon J-M (2010) Philos Trans R Soc London, Ser A 368:3227–3241
2. Manthiram A (2011) J Phys Chem Lett 2:176–184
3. Winter M, Brodd RJ (2004) Chem Rev 104:4245–4270
4. Cheng FY, Liang J, Tao ZL, Chen J (2011) Adv Mater 23:1695–1715
5. Kim T-H, Park J-S, Chang SK, Choi S, Ryu JH, Song H-K (2012) Adv Energy Mater 2:860–872
6. Song HK, Lee KT, Kim MG, Nazar LF, Cho J (2010) Adv Funct Mater 20:3818–3834
7. Mitzushima K, Jones PC, Wiseman PJ, Goodenough JB (1980) Mater Res Bull 15:783–789
8. Nagaura T, Tozawa K (1990) Prog Batteries Sol Cells 9:209
9. Antolini E (2004) Solid State Ionics 170:159–171
10. Tarascon J-M, Armand M (1998) Nature 414:359–367
11. Xia Y, Takeshige H, Noguchi H, Yoshio M (1995) J Power Sources 56:61–67
12. Liu Z, Wang W-L, Liu X, Wu M, Li D, Zhen Z (2004) J Solid State Chem 177:1585–1591
13. Padhi AK, Nanjundaswamy KS, Goodenough JB (1997) J Electrochem Soc 144:1188–1194
14. Chen M, Du C, Song B, Xiong K, Yin G, Zuo P, Cheng X (2013) J Power Sources 223:100–106
15. Yoshida J, Stark M, Holzbock J, Hüsing N, Nakanishi S, Iba H, Abe H, Naito M (2013) J Power Sources 226:122–126
16. Hong J, Wang F, Wang X, Graetz (2013) J Power Sources 196:3659–3663
17. Taniguchi I (2005) Mater Chem Phys 92:172–179
18. Taniguchi I, Song D, Wakihara M (2002) J Power Sources 109:333–339
19. Zhu Z, Yan H, Zhang D, Li W, Lu Q (2013) J Power Sources 224:13–19
20. Xiao L, Guo Y, Qu D, Deng B, Liu H, Tang D (2013) J Power Sources 225:286–292
21. Wang Y, Shao X, Xu H, Xie M, Deng S, Wang H, Liu J, Yan Hui (2013) J Power Sources 226:140–148
22. Kurosumi S, Horiba K, Nagamura N, Kumigashira, Oshima M, Furutsuki S, Nishimura S, Yamada, Mizuno N (2013) J Power Sources 226:42–46
23. Xiao J, Chernova N, Upreti S, Chen X, Li Z, Deng Z, Choi D, Xu W, Nie Z, Graff G, Liu J, Whittingham M, Zhang J (2011) Phys Chem Chem Phys 13:18099–18106
24. Fergus J (2010) J Power Sources 195:939–954
25. Ellis B, Lee K, Nazar L (2010) Chem Mater 22:691–714
26. Xu B, Qian D, Wang Z, Meng Y (2012) J Power Sources 73:51–65
27. Liu J, Zhang J, Yang Z, Lemmon J, Imhoff C, Graff G, Li L, Hu J, Wang C, Xiao J, Xia G, Viswanathan V, Baskaran S, Sprenkle V, Li X, Shao Y, Schwenzer B (2012) Adv Funct Mater. doi:10.1002/adfm.201200690
28. Marom R, Amalraj S, Leifer N, Jacob D, Aurbach D (2011) J Mater Chem 21:9938–9954
29. Etacheri V, Marom R, Elazari R, Salitra G, Aurbach D (2011) Energy Environ Sci 4:3243–3262
30. Su L, Yu J, Zhou Z (2011) Nanoscale 3:3967–3983
31. Cabana J, Monconduit L, Larcher D, Palacín M (2010) Adv Mater 22:E170–E192
32. He P, Yu H, Li D, Zhou H (2012) J Mater Chem 22:3680–3695
33. Bruce P, Scrosati B, Tarascon J (2008) Angew Chem Int Ed 47:2930–2946
34. Li H, Wang Z, Chen L, Huang X (2009) Adv Mater 21:4593–4607
35. Rossen E, Jones CDW, Dahn JR (1992) Solid State Ionics 57:311–318
36. Ohzuku T, Makimura Y (2001) Chem Lett 30:744–745
37. Lu ZH, Macneil DD, Dahn JR (2001) Electrochem Solid-State Lett 4:A191–A194
38. Ohzuku T, Majumura Y (2001) Chem Lett 30:744–745
39. Makimura Y, Ohzuku T (2003) J Power Sources 119–121:156–160
40. Kang K, Meng YS, Breger J, Grey CP, Ceder G (2006) Science 311:977–980
41. Xia H, Tang SB, Lu L (2008) J Alloys Compd 449:296–299
42. Meng XL, Dou SM, Wang WL (2008) J Power Sources 184:489–493
43. Hinuma Y, Meng YS, Kang K, Ceder G (2007) Chem Mater 19:1790–1800
44. Lu Z, MacNeil DD, Dahn JR (2001) Electrochem Solid-State Lett 4:A191–A194
45. Lu Z, Beaulieu LY, Donaberger RA, Thomas CL, Dahn JR (2002) J Electrochem Soc 149:A778–A791
46. Chou J, Kim Y, Kim G (2007) J Phys Chem C 111:3192–3196
47. Zhang B, Chen G, Xu P, Lv Z (2007) Solid State Ionics 178:1230–1234
48. Dou SM, Wang W-L (2011) J Solid State Electrochem 15:399–404
49. Dou SM, Wang W-L, Li HJ, Xin XD (2011) J Solid State Electrochem 15:747–751
50. Sun Y-K, Myung S-T, Park B-C, Prakash J, Belharouak I, Amine K (2009) Nat Mater 8:320–324
51. Kim Y, Cho J, Kim T, Park B (2003) J Electrochem Soc 150: A1723–A1725
52. Cho J, Kim Y, Park B (2001) Electrochem Solid-State Lett 4: A159–A161
53. Cho J, Kim Y, Park B (2000) Chem Mater 12:3788–3791
54. Chang Z, Lv H, Tang H, Li H, Yuan X, Wang H (2009) Electrochim Acta 54:4595–4599
55. Lu C, Fey G, Kao H (2009) J Power Sources 189:155–162
56. Lee K, Myung S, Amine K, Yashiro H, Sun Y (2009) J Mater Chem 19:1995–2005
57. Kang H, Myung S, Amine K, Lee S, Sun Y (2010) J Power Sources 195:2023–2028
58. Landschoot N, Kelder E, Kooyman P, Kwakernaak C, Schoonman J (2004) J Power Sources 138:262–270
59. Miyashiro H, Kobayashi Y, Seki S, Mita Y, Usami A, Nakayama M, Wakihara M (2005) Chem Mater 17:5603–5605
60. Myung S, Amine K, Sun Y (2010) J Mater Chem 20:7074–7095
61. Chen Z, Qin Y, Amine K, Sun Y (2010) J Mater Chem 20:7606–7612
62. Li C, Zhang H, Fu L, Liu H, Wu Y, Rahm E, Holze R, Wu H (2006) Electrochim Acta 51:3872–3883
63. Fu L, Liu H, Li C, Wu Y, Rahm E, Holze R, Wu H (2006) Solid State Sci 8:113–128
64. Guo R, Shi P, Cheng X, Sun L (2009) Electrochim Acta 54:5796–5803
65. Zheng JM, Li J, Zhang ZR, Guo XJ, Yang Y (2008) Solid State Ionics 179:1794–1799
66. Wu F, Wang M, Su Y, Chen S, Xu B (2009) J Power Sources 191:628–632
67. Huang Y, Chen J, Ni J, Zhou H, Zhang X (2009) J Power Sources 188:538–545
68. Hu S-K, Cheng G-H, Cheng M-Y, Hwang B-J, Santhanam R (2009) J Power Sources 188:564–569
69. Kim G-Y, Park YJ, Jung KH, Yang D-J, Lee JW, Kim HG (2008) J Appl Electrochem 38:1477–1481

70. Wu Y, Manthiram A (2009) Solid State Ionics 180:50–56
71. Xiang J, Chang C, Yuan L, Sun J (2008) Electrochem Commun 10:1360–1363
72. Fey GT-K, Chang C-S, Kumar TP (2010) J Solid State Electrochem 4:17–29
73. Gu Y, Chen D, Jiao X, Liu F (2007) J Mater Chem 17:1767–1776
74. Eom J, Cho J (2008) J Electrochem Soc 155:A201–A205
75. Wu Y, Murugan AV, Manthiram A (2008) J Electrochem Soc 155: A635–A641
76. Zeng Y, He J (2009) J Power Sources 189:519–521
77. Kim Y, Hong Y, Ryu KS, Kim MG, Cho J (2008) J Power Sources 179:780–784
78. Sun Y-K, Myung S-T, Park B-C, Yashiro H (2008) J Electrochem Soc 155:A705–A710
79. Kim H-B, Park B-C, Myung S-T, Amine K, Prakash J, Sun Y-K (2008) J Power Sources 179:347–350
80. Sun Y-K, Myung S-T, Yoon CS, Kim D-W (2009) Electrochem Solid-State Lett 12:A163–A166
81. Zheng JM, Zhang ZR, Wu XB, Dong ZX, Zhu Z, Yang Y (2008) J Electrochem Soc 155:A775–A782
82. Lin H, Yang Y (2009) Acta Chemic Sinica 67:104–108
83. Marcinek ML, Wilcox JW, Doeff MM, Kostecki RM (2009) J Electrochem Soc 156:A48–A51
84. Kim H-S, Kim K, Moon SI, Kim I-J, Gu H-B (2008) J Solid State Electrochem 12:867–872
85. Lin B, Wen Z, Han J, Wu X (2008) Solid State Ionics 179:1750–1753
86. Wang GP, Zhang QT, Yu ZL, Qu MZ (2008) Solid State Ionics 179:263–268
87. Eduardo P-C, Yodalgis M, Ricardo M, Milian CR, Sanchez O, Varela JA, Hortencia A, Souza E, Arandad P, Eduado R-H (2008) J Mater Chem 18:3965–3971
88. Liu J, Wang Q, Reeja-Jayan B, Manthiram A (2010) Electrochem Commun 12:750–753
89. Yang Z, Yang W, Evans DG, Zhao Y, Wei X (2009) J Power Sources 189:1147–1153
90. Chen J-M, Cho Y-D, Hsiao C-L, Fey GT-K (2009) J Power Sources 189:279–287
91. Lu C-Z, Chen J-M, Cho Y-D, Hsu W-H, Muralidharana P, Fey GT (2008) J Power Sources 184:392–401
92. Li G, Yang Z, Yang W (2008) J Power Sources 183:741–748
93. Whitacre JF, Zaghib K, West WC, Ratnakumar BV (2008) J Power Sources 177:528–536
94. Kim S-B, Lee KJ, Choi WJ, Kim W-S, Jang IC, Lim HH, Lee YS (2010) J Solid State Electrochem 14:919–922
95. Sun Y-K, Han J-M, Myung S-T, Lee S-W, Amine K (2006) Electrochem Commun 8:821–826
96. Han J-M, Myung S-T, Sun Y-K (2006) J Electrochem Soc 153: A1290–A1295
97. Park B-C, Kim H-B, Myung S-T, Amine K, Belharouak I, Lee S-M, Sun Y-K (2008) J Power Sources 178:826–831
98. Myung S-T, Lee K-S, Yoon CS, Sun Y-K, Amine K, Yashiro H (2010) J Phys Chem C 114:4710–4718
99. Belharouak I, Lu W, Vissers D, Amine K (2006) Electrochem Commun 8:329–335
100. Li H, Zhou H (2012) Chem Comm 48:1201–1217
101. Julien CM (2006) J Appl Phys 100:063511
102. Cushing BL, Goodenough JB (2002) Solid State Sci 4:1487–1493
103. Liu J, Wang A, Reeja-Jayan B, Manthiram A (2010) Electrochem Commun 12:750–753
104. Wilcox JD, Patoux S, Doeff MM (2009) J Electrochem Soc 156: A192–A198
105. Karan NK, Balasubramanian M, Abraham DP, Furczon MM, Pradhan DK, Saavedra-Arias JJ, Thomas R, Katiyar RS (2009) J Power Sources 187:586–590
106. Karan NK, Abraham DP, Balasubramanian M, Furczon MM, Thomas R, Katiyar RS (2009) J Electrochem Soc 156:A553–A562
107. Liu L, Sun K, Zhang N, Yang T (2009) J Solid State Electrochem 13:1381–1386
108. Chen Y, Chen R, Tang Z, Wang L (2009) J Alloys Compd 476:539–542
109. Tang H, Zhao F, Chang Z-R, Yuan X-Z, Wang H (2009) J Electrochem Soc 156:A478–A482
110. Sivaprakash S, Majumder SB (2009) J Alloys Compd 479:561–568
111. Zhang B, Chen G, Xu P, Li CC (2008) J Power Sources 176:325–331
112. Komaba S, Yoshii K, Ogata A, Nakai I (2009) Electrochim Acta 54:2353–2359
113. Zhang B, Chen G, Liang Y, Xu P (2009) Solid State Ionics 180:398–404
114. Zhou F, Zhao X, Lu Z, Jiang J, Dahn JR (2008) Electrochem Solid-State Lett 11:A155–A157
115. Lin Y-K, Lu C-H (2009) J Power Sources 189:353–358
116. Zhou F, Zhao X, Dahn JR (2009) J Electrochem Soc 156:A343–A347
117. Zhou F, Zhao X, Jiang J, Dahn JR (2009) Electrochem Solid-State Lett 12:A81–A83
118. Xiang J, Chang C, Zhang F, Sun J (2009) J Alloys Compounds 475:483–487
119. Xiang J, Chang C, Zhang F, Sun J (2008) J Electrochem Soc 155: A520–A525
120. He Y-S, Pei L, Liao X-Z, Ma Z-F (2007) J Fluorine Chem 128:139–143
121. Croguennec L, Bains J, Menetrier M, Flambard A, Bekaert E, Jordy C, Biensan P, Delmas C (2009) J Electrochem Soc 156: A349–A355
122. Ohzuku T, Makimura Y (2001) Chem Lett 30:642–643
123. Xu B, Qian D, Wang Z, Meng YS (2012) Mater Sci Eng R 73:51–65
124. Yabuuchi N, Ohzuku T (2005) J Power Sources 146:636–639
125. Shaju KM, Bruce PG (2006) Adv Mater 18:2330–2334
126. Li Z, Chernova NA, Roppolo M, Upreti S, Petersburg C, Alamgir FM, Whittingham MS (2011) J Electroche Soc 158:A516–A522
127. Sivaprakash S, Majumder SB, Katiyar RS (2009) J Electrochem Soc 156:A328–A333
128. Thackeray MM, Kang S-H, Johnson CS, Vaughey JT, Benedek R, Hackney SA (2007) J Mater Chem 17:4012–4016
129. Johnson CS, Li N, Lefief C, Vaughey JT, Thackeray MM (2008) Chem Mater 20:6095–6106
130. Kim G-Y, Yi S-B, Park YJ, Kim H-G (2008) Mater Res Bull 43:3543–3552
131. Guo X-J, Li Y-X, Zheng M, Zheng J-M, Li J, Gong Z-L, Yang Y (2008) J Power Sources 184:414–419
132. Yabuuchi N, Yoshii K, Myung S-T, Nakai I, Komaba S (2011) J Am Chem Soc 133:4404–4419
133. Kang S-H, Thackeray MM (2008) J Electrochem Soc 155:A269–A275
134. Gao J, Manthiram A (2009) J Power Sources 191:644–647
135. Lim J-H, Bang H, Lee K-S, Amine K, Sun Y-K (2009) J Power Sources 189:571–575
136. Shi SJ, Tu JP, Tang YY, Yu YX, Zhang YQ, Wang XL, Gu CD (2013) J Power Sources. doi:10.1016/j.jpowsour.2012.11.091
137. Zhao T, Chen S, Li L, Zhang X, Chen R, Belharouak I, Wu F, Amine K (2013) J Power Sources. doi:10.1016/j.jpowsour.2012.11.099
138. Kosova NV, Devyatkina ET, Kaichev VV (2009) Russ J Electrochem 45:277–285
139. Thackeray MM, Kang SH, Johnson CS, Vaughey JT, Benedek R, Hackney SA (2007) J Mater Chem 17:3053–3272
140. Johnson CS, Li N, Lefief C, Thackeray MM (2007) Electrochem Commun 9:787–795

141. AricQ AS, Bruce P, Scrosati B, Tarascon J-M, Van Schalkwijc W (2005) Nat Mater 4:366–377
142. Balaya P, Bhattacharyya AJ, Jamnik J, Zhukovskii YF, Kotomin EA, Maier J (2006) J Power Sources 159:171–178
143. Bruce PG, Scrosati B, Tarascon J-M (2008) Angew Chem Int Ed 47:2930–2946
144. Pitchai R, Thavasi V, Mhaisalkarb SG, Ramakrishna S (2011) J Mater Chem 21:11040–11051
145. Hong Y-S, Park YJ, Ryu KS, Chang SH, Kim MG (2004) J Mater Chem 14:1424–1429
146. Cho J, Kim Y, Kim MG (2007) J Phys Chem C 111:3192–3196
147. Kim MG, Joi M, Hong Y-S, Cho J (2009) Chem Commun:218–220
148. Yang C, Huang J, Huang L, Wang G (2013) J Power Sources 226:219–222